Midbrain volume segmentation using Active Shape Models and LBPs

Jimena Olveres[a], Rodrigo Nava[a], Boris Escalante-Ramírez[b], Gabriel Cristóbal[c], and Carla María García-Moreno[d]

[a] Posgrado en Ciencia e Ingeniería de la Computación, Universidad Nacional Autónoma de México, Mexico City, Mexico.
[b] Departamento de Procesamiento de Señales, Facultad de Ingeniería, Universidad Nacional Autónoma de México, Mexico City, Mexico.
[c] Instituto de Óptica, Spanish National Research Council (CSIC), Serrano 121, Madrid 28006, Spain.
[d] Hospital Ángeles Lomas, State of Mexico, Mexico.

ABSTRACT

In recent years, the use of Magnetic Resonance Imaging (MRI) to detect different brain structures such as midbrain, white matter, gray matter, corpus callosum, and cerebellum has increased. This fact together with the evidence that midbrain is associated with Parkinson's disease has led researchers to consider midbrain segmentation as an important issue. Nowadays, Active Shape Models (ASM) are widely used in literature for organ segmentation where the shape is an important discriminant feature. Nevertheless, this approach is based on the assumption that objects of interest are usually located on strong edges. Such a limitation may lead to a final shape far from the actual shape model. This paper proposes a novel method based on the combined use of ASM and Local Binary Patterns for segmenting midbrain. Furthermore, we analyzed several LBP methods and evaluated their performance. The joint-model considers both global and local statistics to improve final adjustments. The results showed that our proposal performs substantially better than the ASM algorithm and provides better segmentation measurements.

Keywords: Active Shape Models, Dice's coefficient, Hausdorff distance, Local Binary Patterns, Midbrain segmentation

1. INTRODUCTION

Midbrain or mesencephalon is an approximately 2×2×1 cm sized region near the center of the brain that serves as a relay center for visual, auditory, and motor system information. It controls many important functions such as pupil diameter, eye movement, and hearing. Two structures can be identified in the interior of the midbrain: the *red nucleus*, which is involved in motor coordination and the *substantia nigra*, a dark area related to learning process and motor control.[1] The *substantia nigra* contains high levels of melanin and dopamine-containing neurons, which are severely affected by the degenerative process of Parkinson's disease (PD).[2]

In 2010, Sakal et al.[3] proposed a technique based on echoscopy for supporting the clinical diagnosis of PD; they have claimed that the initial assessment of the neurological condition of a patient should be performed by estimating the area of the *substantia nigra*. A recent non-invasive tool for analyzing midbrain is MRI, which offers the possibility of a deeper study of this organ by obtaining a series of images with the capability to segment and build a volume or a 3D representation. However, visualization of inner structures, which helps diagnosis of PD, can not be achieved so easily. Chen et al.[4] addressed this issue and proposed affine registration of two modalities of MRI: T1 and SWI.

Further author information:
J.O.: E-mail: jolveres@uxmcc2.iimas.unam.mx

Applications of Digital Image Processing XXXVI, edited by Andrew G. Tescher,
Proc. of SPIE Vol. 8856, 88561F · © 2013 SPIE · CCC code: 0277-786X/13/$18
doi: 10.1117/12.2024396

Precisely, because of the fact that PD is associated with destruction of neurons in the midbrain, its segmentation has become an important issue in neurological applications. Currently, midbrain segmentation is a manual process where experts delineate the contours of the organ from MRI images. State-of-the-art approaches to segment midbrain automatically are mainly based on active models applied on ultrasound and sonographic modalities.[5,6] These studies use different variants of Active Contour Models (ACM) and Active Appearance Models (AAM) and even make use of the toolbox SPHARM.[7] However, automatic segmentation of the midbrain and *substantia nigra* area still poses a challenge. One important drawback is the lack of databases available for this type of research.

Midbrain normally has a typical shape which can be obtained by statistical methods. Nevertheless, noise and lack of contrast are two frequently problems that hamper the final segmentation. To overcome this issue, this paper proposes an automatic method for segmenting midbrain based on the combined use of Active Shape Models (ASM) and Local Binary Patterns (LBP). The joint-model considers both global and local statistics to improve the final shape. We use LBPs to detect midbrain boundaries correctly; LBPs add to ASMs the robustness needed to detect non-salient boundaries in the presence of noise that some other methods lack.[8] The result was a statistical model able to improve structure resolution because of the LBPs.

This paper is organized as follows: the first part is devoted to describe the ASM and LBPs techniques. In Section 2 the dataset is described, then in Section 3 we present our approach. Later, in Section 4 we show our results with the improvements obtained. Finally the conclusions are drawn in Section 5.

1.1 Active shape models

Active Shape Models[9] are part of the statistical deformable models; they can detect specific shape boundaries such as midbrain. Cootes et al. argue that a shape model can deform to some extent within a certain variability. Therefore, ASMs are able to deform their shape so that they resemble the real organ. Other studies[8,10,11] have applied ASMs to different anatomical organs, such as heart and pediatric cerebellum.

ASMs need a training set of aligned shapes of an object using pose transformations (rotation, translation, and scaling). The shapes can be modeled as follows:

$$\hat{X} = \bar{X} + P\boldsymbol{b} \tag{1}$$

where $\bar{X} = \frac{1}{s}\sum_{i=0}^{s-1} x_i$ is the mean shape, P is the matrix of the t first principal components, b is a vector of weights and $\hat{X}$ is the estimated shape. The previous equation is know as Point Distribution Model (PDM).

It is possible to generate new shapes by modifying b within certain limits to obtain similar shapes of the object to be recognized.[12] The algorithm consists basically of two steps: **build a statistical model** from initial shapes and compute a gray level profile model to obtain specific characteristics of boundary points; and **ASMs search**, where it recognizes a similar model shape.

- **Step (1)** is done by obtaining a statistical shape and a gray-level profile model. We use manual annotations for each volume to be involved in the training phase, delineating contour lines of the midbrain shape for each image. An alignment is applied to each shape involving translation, rotation, and size transformations. The aligned positions of each landmark in each image slice are grouped into a vector, as follows;

$$S_i = (x_0, y_0, \ldots, x_{n-1}, y_{n-1})^T \tag{2}$$

  After this step, we use single value decomposition[13] to find all the parameters that assemble the Point Distribution Model (PDM) of the data. The number of training datasets is often (very) small in comparison to the number of landmarks and can lead to a singular correlation matrix and over-fitting of the training data. To reduce such effects it is necessary to crop the number of eigenvalues keeping between 90% and 99.5% of the variance in the training data. This is done by removing the lowest eigenvalues and corresponding eigenvectors computed for the PCA analysis.

  The gray-level profile model is also part of the training statistical model construction. Since shapes are described by points enclosing a contour, gray-level profiles normal to each landmark point are calculated.

First and second moments are obtained by calculating the mean and covariance matrix from the training set. Either the gray profile or its normalized derivative can be employed. Using derivatives of the gray profile may be advantageous because it avoids the problem of contrast invariance in the images but, at the same time they are more sensitive to noise.[8]

- **Step (2)** is the ASM search within the PDM obtained on the previous phase. The mean shape is deformed to recognize a new shape. First, we position the mean object shape close to the object in the image manually. Each point of the mean form is compared against the point in the correspondent profile and the landmark points are moved iteratively towards those that obtain the lowest distance, using for example, the Mahalanobis distance. Using these points, we modify the initial shape using Eq. (1).

  The new contour coordinates, $\hat{X}$, are an estimate of the original contour, $\bar{X}$. Here, b is constrained to the range $\pm m\sqrt{\lambda_i}$ with m between 2 and 3. This restriction limits shapes within 2 or 3 standard deviations of the distribution of shapes in the training data.

  Finally, all boundary points move into the direction of the least distance. When new positions for the landmarks are found, an aligning process must be computed to adjust the shape. Pose parameters are used to calculate final deformations to move the current estimate to a new position. The process is iterative and it continues until reaching a specific number of iterations or threshold.

1.2 Local binary patterns

- The original **Local Binary Pattern** (LBP) descriptor[14] was proposed by Ojala et al. It is based on the idea that textural properties within homogeneous regions can be mapped into patterns that represent micro-features. This proposal uses a fixed rectangular 3×3 mask, which represents a neighborhood around a central pixel. The values within the rectangular mask are compared with their central pixel; those ones lesser than the central value are labeled with "0" otherwise they are labeled with "1". The labeled pixels are multiplied by a weighting function according with their positions to form a pattern chain. Afterwards, the sum of the eight pixels replaces the value of the central pixel. This method describes differences of intensities and produces 2^8 possible labels. In addition, it has very low computational and space complexity. Ojala et al. have claimed that this type of threshold operations provide a robust way for describing local texture patterns.

  Further generalizations use a circular neighborhood instead of a fixed rectangular region. The sampling coordinates of the neighbors are calculated using the expression: $(x_c + R\cos[\frac{2\pi p}{P}], y_c - R\sin[\frac{2\pi p}{P}])$. If a coordinate does not fall on an integer position then the intensity values are bi-linearly interpolated. Such implementations allow us choosing the spatial resolution (R) and the number of sampling points (P) as follows:

$$LBP_{P,R}(g_c) = \sum_{p=0}^{P-1} s(g_p - g_c)\, 2^p \tag{3}$$

  where P is the number of sampling points, R represents the radius of the neighborhood, g_c, is the central pixel at (x_c, y_c), and $\{g_p | p = 0, \ldots, P-1\}$ are the values of the neighbors whereas the comparison function, $s(x)$, is defined as:

$$s(x) = \begin{cases} 1 & \text{if } x \geq 0 \\ 0 & \text{if } x < 0 \end{cases} \tag{4}$$

- **Uniform Local Binary Patterns** ($LBP^{uni}_{P,R}$).[15] Over 90% of LBP texture patterns can be described with few spatial transitions, which are the changes (0/1) in a pattern chain. Ojala et al. introduced a measure of uniformity, $U(LBP_{P,R}(g_c)) = |s(g_{p-1} - g_c) - s(g_0 - g_c)| + \sum_{p=1}^{P-1} |s(g_p - g_c) - s(g_{p-1} - g_c)|$, which corresponds to the number of spatial transitions. So that, $LBP^{uni}_{P,R}$ can be obtained as:

$$LBP^{uni}_{P,R}(g_c) = \begin{cases} \sum_{p=0}^{P-1} s(g_p - g_c) & \text{if } U(LBP_{P,R}(g_c)) \leq 2 \\ P+1 & \text{otherwise} \end{cases} \tag{5}$$

then, the pixel-wise information is encoded as a histogram, H_i, so that it can be interpreted as a fingerprint or a signature of the analyzed object.

- Yan Ma[16] proposed the **Number LBP** ($LBP^{num}_{P,R}$) as an extension of the Eq. (5) by dividing the non-uniform patterns into groups based on the number of "1" or "0" bits as follows:

$$LBP^{num}_{P,R}(g_c) = \begin{cases} \sum_{p=0}^{P-1} s(g_p - g_c) & \text{if } U(LBP_{P,R}(g_c)) \leq 2 \\ Num_1\{LBP_{P,R}(g_c)\} & \text{if } \begin{array}{l} U(LBP_{P,R}) > 2 \quad \text{and} \\ Num_1\{LBP_{P,R}(g_c)\} \geq Num_0\{LBP_{P,R}(g_c)\} \end{array} \\ Num_0\{LBP_{P,R}(g_c)\} & \text{if } \begin{array}{l} U(LBP_{P,R}) > 2 \quad \text{and} \\ Num_1\{LBP_{P,R}(g_c)\} < Num_0\{LBP_{P,R}(g_c)\} \end{array} \end{cases} \tag{6}$$

  where $Num_1\{\bullet\}$ is the number of "1" and $Num_0\{\bullet\}$ is the number of "0" in the non-uniform pattern.

- The presence of noise can seriously impair the performance of the LBP operator. Zabih's proposal[17] replaces the central pixel with the median of itself and the P neighbors. This implementation is called **median LBP**.

$$LBP^{med}_{P,R}(g_c) = \sum_{p=0}^{P-1} s(g_p - \widetilde{g}) \tag{7}$$

  where $\widetilde{g}$ represents the median of the P neighbors and the central pixel. This modification is still invariant to rotation but less sensitive to noise. It is also invariant to monotonic illumination changes.

Keomany and Marcel[18] proposed a method that combines ASM and LBP using what is known as Extended LBP and Square-based LBP. They concluded to have better results with the ASM/LBP approach than with the ASM algorithm alone.

2. MATERIALS

In our experiments we used a dataset labeled by an experienced image neurologist. This dataset was selected randomly by Dr. García at Hospital Interlomas (Mexico) using CT scans. It consists of cranial annotated midbrain studies from 10 normal subjects. The T2 images were obtained on a 3 Tesla scanner, (TR = 3200 ms, TE = 409ms, flip angle = 120), obtaining volumes of 512 × 448 × 176 pixels with a resolution of 0.44921 × 0.44921 × 0.9 mm.

The volume images were preprocessed with a normalization of gray intensities and our area of interest is approximately 70 × 70 pixels per image. The algorithms were run on a Intel Xeon Quad Core workstation with 2.40Ghz and 6GB of RAM memory.

3. PROPOSED METHOD

Our proposal aims to evaluate different combinations of ASM/LBP algorithms, and at the same time improve midbrain segmentation. We also tested the simple ASM algorithm in order to have a comparison base for our improvements. We used cranial magnetic resonance images containing the midbrain volume. One of the main problems we found was the lack of sufficient data in order to train the ASM according to the estimates mentioned by Cootes. At the moment, we have 10 segmented volumes and opted for the method of Leave One Out. The computed ASM/LBP algorithm differs from Keomany in the way that they first obtained their LBP's image and then apply the ASM Algorithm.

In our proposal, for the **training phase**, the LBP operator evaluates each landmark point on a window of 5×5 pixels. This is accomplished instead of the gray profiles of the traditional method. An LBP analysis is computed for each pixel of the window. The result is a characteristic histogram of the surrounded region of the landmarks. This fact implies that instead of evaluating over one central pixel, the LBP evaluates over a whole region. Hence, more information of the area is saved in the training phase and used for recognition.

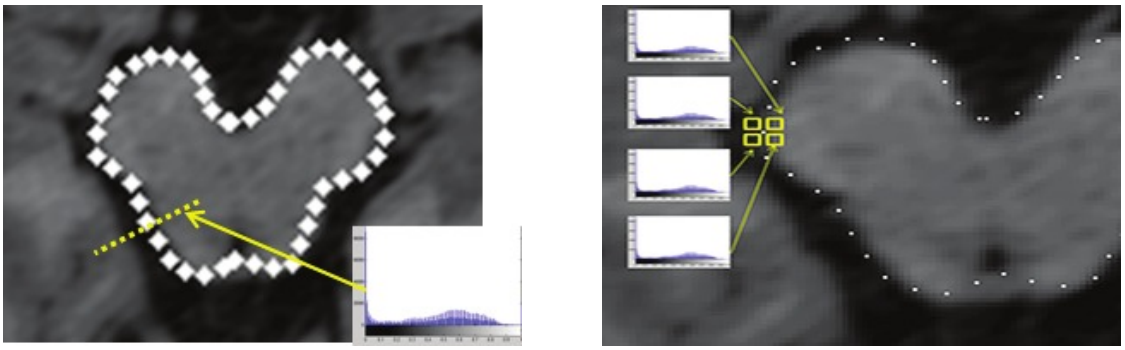

(a) (b)

Figure 1. Two different ways to combine LBPs with ASMs. **(a)** LBP's histogram for each profile landmark of the contour; and **(b)** Quadratic LBP's histogram for each contour landmark.

In the **ASM search** we evaluated the LBP's normal profiles of the contour, see Fig. 1(a), and used it to obtain the correct boundary adjustment.

A second approach, is to take into account a bigger divided quadratic region, where the central pixel is the landmark point and its surrounding area is divided into 4 windows of size 5×5 pixels and an LBP was computed for each window. Resulting histogram of each quadratic zone is concatenated to produce a single one, see Fig. 1(b).

Both methods take into account the original ASM's profile-based search but instead of getting a distance of the gray values or combination of derivative gray values, the histograms are compared against the one of the PDM training model. Chi distance is used to compute similarities between the new test object histogram, H and the training histogram, $\bar{H}$. The smallest distance is where the point boundary moves. The smaller the distance, the more similar is the test region where the boundary is located, and it leads to a better segmentation as follows:

$$X^2\left(H,\bar{H}\right)=\sum_i \frac{\left(H_i-\bar{H}_i\right)^2}{\left(H_i+\bar{H}_i\right)} \tag{8}$$

The simplest algorithm starts by obtaining the profile of the landmark point and then calculates its LBP for each profile point. The point with the smallest Chi distance is to where the contour moves.

In addition, we also evaluated the behavior of three LBP techniques: the uniform LBP, Eq. (5), the number LBP, Eq. (6), and the median LBP, Eq. (7) with the ASM to compare their performance with the simple LBP defined in the Eq. (3). The LBP methods performs a 360 degrees calculus of each pixel inside the evaluated area. This means that all the pixels supply component values to the resulting histogram, independently if it is profile or divided quadratic region. The result is a more thorough histogram of the gray values existent within the area.

4. EXPERIMENTAL RESULTS

The proposal was evaluated on 10 slices of the midbrain volume using both the ASM/LBP profile and ASM/LBP quadratic schemes explained in the previous section. Once the volume is segmented, we can compare the results against the expert segmented data. We used the Dice index, Eq. (9), and Hausdorff distance, Eq. (10), as our comparison measure, and obtained a value for each ASM/LBP scheme and for the ASM algorithm, as well as for each slice of the volume. The Dice index, d_D, uses the intersected area between the expert and recognized contours divided by the sum of both areas. The result is a normalized value between 0 and 1 that indicates how similar are both contours. The closest the value is to 1 the more similar the shapes are. The equation is defined as follows:

$$d_D=\frac{2\times(\|A\cap B\|)}{(\|A\|+\|B\|)} \tag{9}$$

Table 1. Dice index and Hausdorff distance for the classic ASM. Dice value is between 0 and 1, values close to 1 indicate more similar contours. On the contrary, Hausdorff minimal values indicate more alike boundaries in a range from 0 to 100. Bold values are the best values.

	ASM	
slice	Dice	Haussdorf
1	0.6619	18.3033
2	0.8441	13.0832
3	0.6652	18.4192
4	0.8342	9.5777
5	**0.8984**	9.7526
6	0.4632	25.6629
7	0.5044	19.6673
8	0.4604	34.0986
9	0.7563	14.6582
10	0.8833	**8.0058**
$\mu(\sigma)$	0.6971 ($\pm$0.1730)	17.1229($\pm$8.0789)

The Hausdorff distance, d_H, measures how close a point from a first set is from another point of the second set in a metric space –in our case between two sets of points, P and Q (or boundaries). It is defined as follows:

$$d_H(P,Q) = \max\{d(P,Q),\, d(Q,P)\} \tag{10}$$

where $d(P,Q) = \min\{\|p_{max} - q\| \, |p_{max} \in \max\{\|p - q\|\},\, q \subset Q,\, p \subset P\}$; intuitively, $d(P,Q)$ finds the p point from the set P that is the farthest from any point in Q and measures the distance from p to its closest neighbor in Q.

Table 1 shows both Dice index and Hausdorff metric for the ASM algorithm. Note that the slice 8 provided the largest error.

Table 2 and Table 3 summarize the results of Dice index and Hausdorff metric obtained for the profile ASM/LBP scheme, respectively; whereas Table 4 and Table 5 summarize the results of Dice index and Hausdorff metric obtained for the quadratic ASM/LBP scheme, respectively.

Fig.2 to Fig.4 show as a representative set, the resulted segmentation for slice 4 on each of the proposed methods.

One remark from this research is that while the ASM sometimes fails due to the lack of enough training set and parameters variance, the ASM/LBP improves its result with more certainty and less iterations. This is due to the deeper analysis of the surrounding texture of the boundary and the way we move the final points to the desired boundary.

In both cases, profile and quadratic schemes, the join model provides a better adjustment starting from the initial iterations. And it does not need as many initial training data and/or diminishes the number of iterations compared to the traditional ASM.

5. CONCLUSIONS

In this paper we proposed a novel algorithm based on ASMs that incorporates the use of LBPs in order to obtain a better segmentation of midbrain volumes. We used four different LBP approaches: original LBP, uniform LBP, numeric LBP, and median LBP. We compared their performance using midbrain's Magnetic Resonance images. We obtained the best results using first the quadratic LBP algorithm, second the profile LBP, and lastly the

Table 2. Dice index for the profile ASM/LBP scheme using the original LBP, uniform LBP, number LBP, and median LBP. Dice value is between 0 and 1, values close to 1 indicate more similar contours. Bold values are the best per slice

slice	ASM/LBP	ASM/$LBP^{uni}_{P,R}$	ASM/$LBP^{num}_{P,R}$	ASM/$LBP^{med}_{P,R}$
1	0.9500	0.9468	0.9359	**0.9535**
2	0.9376	**0.9474**	0.9434	0.9066
3	**0.9494**	0.9441	0.9199	0.9452
4	**0.9661**	0.9497	0.9456	0.9618
5	**0.9469**	0.9353	0.9363	0.8658
6	**0.9605**	0.8851	0.8856	0.9560
7	**0.9391**	0.9357	0.9305	0.7320
8	**0.9162**	0.5949	0.7149	0.8921
9	0.9183	0.8918	0.6572	**0.9478**
10	0.9294	0.8878	0.8953	**0.9391**
$\mu\,(\sigma)$	0.9414(±0.0166)	0.8919(±0.1076)	0.8765(±0.1032)	0.9100(±0.0700)

Table 3. Hausdorff distance for the profile ASM/LBP using the original LBP, uniform LBP, number LBP, and median LBP. Hausdorff minimal values indicate more similar boundaries in a range from 0 to 100. Bold values are the best per slice.

slice	ASM/LBP	ASM/$LBP^{uni}_{P,R}$	ASM/$LBP^{num}_{P,R}$	ASM/$LBP^{med}_{P,R}$
1	4.1192	4.1700	5.2757	**3.8092**
2	5.9364	**4.8623**	5.1902	8.8964
3	4.8918	5.0158	**4.7317**	6.0091
4	3.6711	**3.5921**	4.1921	3.9940
5	6.2651	6.6675	**5.7891**	9.8802
6	**3.0250**	9.7428	9.2893	3.5945
7	4.9680	5.0747	**4.6684**	19.2409
8	6.7452	19.5279	22.1255	**6.5264**
9	7.5991	7.4235	25.5559	**5.4839**
10	5.7470	6.6885	9.6796	**4.1478**
$\mu\,(\sigma)$	5.2968(±1.4303)	7.2765(±4.6658)	9.6498(±7.7566)	7.1582(±4.7602)

Table 4. Dice index for the quadratic ASM/LBP scheme using the original LBP, uniform LBP, number LBP, and median LBP. Dice value is between 0 and 1, values close to 1 indicate more similar contours. Bold values are the best per slice

slice	ASM/LBP	ASM/$LBP^{uni}_{P,R}$	ASM/$LBP^{num}_{P,R}$	ASM/$LBP^{med}_{P,R}$
1	0.9561	**0.9583**	0.9517	0.9567
2	0.9518	0.9475	0.9513	**0.9527**
3	**0.9479**	0.9476	0.9294	0.9318
4	**0.9642**	0.9583	0.9636	0.9628
7	0.9382	**0.9393**	0.8729	0.9382
6	0.9605	**0.9619**	0.9499	0.9615
7	0.9445	0.9407	0.7624	**0.9458**
8	**0.9212**	0.9188	0.9201	0.9199
9	**0.9405**	0.9278	0.9352	0.9399
10	**0.9563**	0.9539	0.9515	0.9562
$\mu\,(\sigma)$	0.9481($\pm$0.0127)	0.9454($\pm$0.0140)	0.9188($\pm$0.0607)	0.9465($\pm$0.0140)

Table 5. Hausdorff distance for the quadratic ASM/LBP scheme using the original LBP, uniform LBP, number LBP, and median LBP. Hausdorff minimal values indicate more similar boundaries in a range from 0 to 100. Bold values are the best per slice.

slice	ASM/LBP	ASM/$LBP^{uni}_{P,R}$	ASM/$LBP^{num}_{P,R}$	ASM/$LBP^{med}_{P,R}$
1	3.6333	**3.5421**	3.9367	3.6419
2	**4.4091**	4.8927	4.5428	4.4132
3	**4.8565**	4.8846	6.9014	6.6213
4	4.2445	**3.6494**	4.3348	4.3230
7	7.2998	**7.2816**	10.5637	7.3323
6	3.0449	2.9318	3.7003	**2.9285**
7	5.5052	**4.9878**	19.3020	5.4087
8	5.9460	**5.8914**	5.9556	5.9516
9	5.9939	5.8320	**5.2831**	5.9601
10	4.4261	**4.3020**	4.9274	4.5939
$\mu\,(\sigma)$	4.9359($\pm$1.2626)	4.8195($\pm$1.2956)	6.9448($\pm$4.7815)	5.1174($\pm$1.3755)

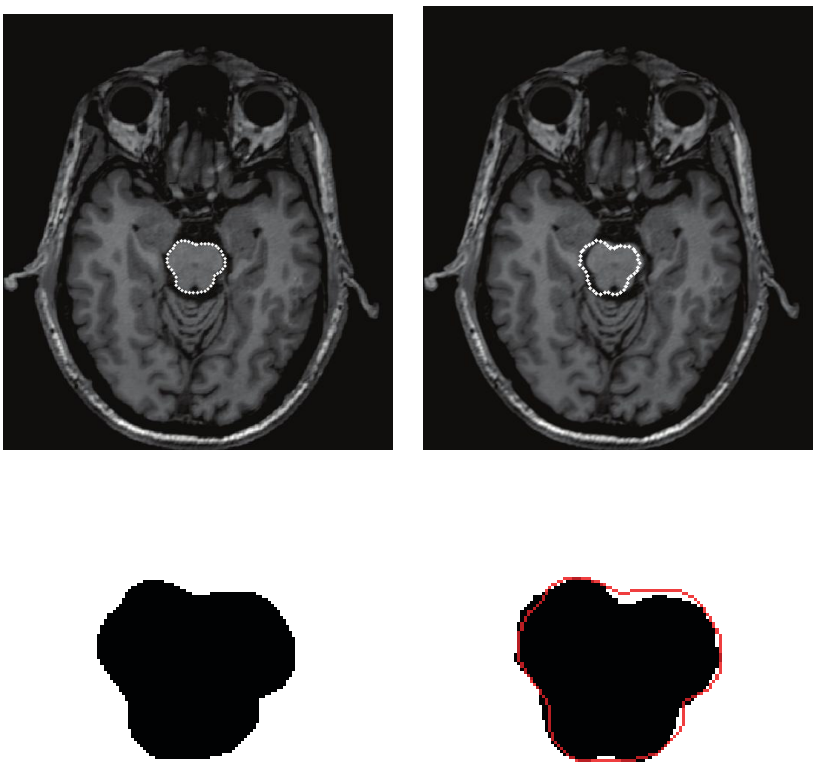

(a) (b)

Figure 2. Cranial MR images; the first row shows axial original view and second row shows binary midbrain segmentation; binary images were augmented 2X for a better visualization. **(a)** expert annotated boundary; and **(b)** classic ASM recognized boundary; the red contour in binary image indicates the expert boundary.

(a) (b) (c) (d)

Figure 3. Profile ASM/LBP scheme midbrain segmentation; binary images were augmented 2X for a better visualization. The red contour indicates the expert boundary. **(a)** ASM/LBP; **(b)** ASM/LBPuni; **(c)** ASM/LBPnum; and **(d)** ASM/LBPmed

(a) (b) (c) (d)

Figure 4. Quadratic ASM/LBP scheme midbrain segmentation; binary images were augmented 2X for a better visualization. The red contour indicates the expert boundary. **(a)** ASM/LBP; **(b)** ASM/LBPuni; **(c)** ASM/LBPnum; and **(d)** ASM/LBPmed

classic ASM method. We also can notice that in the case of the profile ASM/LBP scheme the semiautomatic process for the initial position is very important and can vary the results, which did not happen in the quadratic ASM/LBP scheme. For the ASM, this fact causes not to converge correctly. Even though we did not have enough data to test the algorithm, the quadratic ASM/LBP shows a major performance compared to the other methods. This is due to the fact that a bigger area that characterizes the midbrain contour is analyzed.

Further research will be devoted to test the algorithm with different data, such as midbrain's volumes with deformations or degenerative problems that affect the final shape.

ACKNOWLEDGMENTS

This work has been sponsored by the grant UNAM PAPIIT IN113611. R. Nava and J. Olveres give a special thank to Consejo Nacional de Ciencia y Tecnología for the doctoral scholarships 167161 and 70011, respectively.

REFERENCES

[1] Berretta, N., Bernardi, G., and Mercuri, N. B., "Firing properties and functional connectivity of substantia nigra pars compacta neurones recorded with a multi-electrode array in vitro," *The Journal of Physiology* **588**(10), 1719–1735 (2010).

[2] Damier, P., Hirsch, E. C., Agid, Y., and Graybiel, A. M., "The substantia nigra of the human brain: I. Nigrosomes and the nigral matrix, a compartmental organization based on calbindin D28K immunohistochemistry," *Brain* **122**(8), 1421–1436 (1999).

[3] Sakalauskas, A., Lukosevicius, A., and Lauckaité, K., "Transcranial echoscopy for diagnostic of Parkinson disease: technical constraints and possibilities," *Ultragarsas* **65**, 47–50 (2010).

[4] Chen, J., Khan, A. R., Denk, C., Galley, S., Rauscher, A., McKeown, M., and Beg, M., "Multistructure registration allows group interpretation of midbrain iron content in Parkinsonś," in [*16th Annual Meeting of the Organization for Human Brain Mapping*], (2010).

[5] Engel, K. and Toennies, K., "Segmentation of the midbrain in transcranial sonographies using a two-component deformable model," *Annals of the BMVA* **2009**, 1–13 (2009).

[6] Kier, C., Cyrus, C., Seidel, G., Hofmann, U. G., and Aach, T., "Segmenting the substantia nigra in ultrasound images for early diagnosis of Parkinson's disease," *International Journal of Computer Assisted Radiology and Surgery* **2**, S83–S85 (June 2007).

[7] Shen, L., Farid, H., and McPeek, M. A., "Modeling three-dimensional morphological structures using spherical harmonics," *Evolution* **63**(4), 1003–1016 (2009).

[8] Barba-J., L., Olveres, J., Escalante-Ramírez, B., Arámbula, F., and Vallejo, E., "Segmentation of 4D cardiac computer tomography images using active shape models," in [*Proc. SPIE 8436, Optics, Photonics, and Digital Technologies for Multimedia Applications II*], 84361E–11 (2012).

[9] Cootes, T. F., Taylor, C. J., Cooper, D. H., and Graham, J., "Active shape models: their training and application," *Comput. Vis. Image Underst.* **61**(1), 38–59 (1995).

[10] Becker, B. G., Cosío, F. A., Huerta, M. E. G., and Benavides-Serralde, J. A., "Automatic segmentation of the cerebellum of fetuses on 3D ultrasound images,using a 3D point distribution model," in [*Annual International Conference of the IEEE Engineering in Medicine and Biology Society.*], 4731–4 (2010).

[11] Faghih Roohi, S. and Aghaeizadeh Zoroofi, R., "4D statistical shape modeling of the left ventricle in cardiac MR images," *International Journal of Computer Assisted Radiology and Surgery* **8**(3), 335–351 (2013).

[12] Abu-gharbieh, R., Hamarneh, G., and Gustavsson, T., "Review - active shape models - part ii: Image search and classification," in [*In Proc. Swedish Symposium on Image Analysis*], 129–132 (1998).

[13] Kroon, D. J., *Segmentation of the Mandibular Canal in Cone-Beam CT Data*, PhD thesis, University of Twente (December 2011).

[14] Ojala, T., Pietikainen, M., and Harwood, D., "Performance evaluation of texture measures with classification based on Kullback discrimination of distributions," in [*Proceedings of the 12th International Conference on Pattern Recognition - Conference A: Computer Vision Image Processing (IAPR)*], **1**, 582–585 (1994).

[15] Ojala, T., Pietikäinen, M., and Mäenpää, T., "Multiresolution gray-scale and rotation invariant texture classification with local binary patterns," *IEEE Trans. Pattern Anal. Mach. Intell.* **24**(7), 971–987 (2002).

[16] Ma, Y., "Number local binary pattern: An extended local binary pattern," in [*2011 International Conference on Wavelet Analysis and Pattern Recognition (ICWAPR)*], 272 –275 (2011).

[17] Zabih, R. and Woodfill, J., "Non-parametric local transforms for computing visual correspondence," in [*Proceedings of the third European conference on Computer Vision (Vol. II)*], 151–158, Springer-Verlag New York, Inc., Secaucus, NJ, USA (1994).

[18] Keomany, J. and Marcel, S., "Active Shape Models Using Local Binary Patterns," tech. rep., IDIAP (2006).